Science of Sintering, **54** (2022) 295-303

https://doi.org/10.2298/SOS2203295S

UDK: 685.34.036; 535.37

Structural and Luminescence Properties of $SrGd_2O_4$ Nanocrystalline Phosphor Doped with Dy^{3+} and Sm^{3+}

Tijana Stamenković[1], Nadežda Radmilović[1], Marko Nikolić[2], Jelena Erčić[3], Vesna Lojpur[1*)]

[1]Department of Atomic Physics, Vinča Institute of Nuclear Sciences, National Institute of the Republic of Serbia, P.O. Box 522, 11001 Belgrade, University of Belgrade, Serbia

[2]Institute of Physics Belgrade, University of Belgrade, Belgrade, Serbia

[3]Department of Materials, Vinča Institute of Nuclear Sciences, National Institute of the Republic of Serbia, P.O. Box 522, 11001 Belgrade, University of Belgrade, Serbia

Abstract:

In this manuscript, down-conversion nanopowders of $SrGd_2O_4$ doped with different concentrations of either Dy^{3+} or Sm^{3+} ions were examined in detail. All samples were prepared via glycine-assisted combustion method, primarily burned at 500ºC for 1.5 h and additionally calcined at 1000ºC for 2 h, at ambient room temperature. The XRD analysis showed that all samples crystallize as single phase and the orthorhombic lattice $SrGd_2O_4$. TEM analysis determined high degree of crystallinity of samples with grain size of approximately 200 nm for Dy^{3+} doped and 150 nm for Sm^{3+} doped $SrGd_2O_4$. For both samples SAED confirmed that diffraction rings correspond to the hkl plane indices of $SrGd_2O_4$, while EDS confirmed presence of Dy in crystal structure. Results of luminescent characterization demonstrated all appropriate emission peaks related to either Dy^{3+} or Sm^{3+} dopant ions. Investigation of dopant concentration revealed that the lowest values of both dopants have the most prominent emission peaks, while coordinates obtained from the CIE diagram showed emission shifting with the change of concentration.

Keywords*: Down-conversion; Luminescence; $SrGd_2O_4$; Combustion synthesis.*

1. Introduction

Rare earth luminescent materials have attracted immense attention over the last few decades due to the electronic configuration of the rear earths ($4f^n5d^m6s^2$ (n=1–14, m= 0–1)) that gives these phosphors their unique optic, electric and magnetic properties [1]. Possibilities for rare earth phosphors implementation are vast, since they can be used in a wide range of applications, such as temperature sensors, full-color displays, photoelectric devices, solar cells, multimodal imaging probes, heavy metal ion detection etc [2]. Various compounds (oxides, phosphate, fluoride, molybdate, vanadate etc.) are used as host i.e. matrix for experimenting with the creation of new forms of phosphors [3]. Amongst all of the possibilities, oxide-based materials have been found to be very suitable as hosts since they have shown to greatly improve luminescent characteristics such as emission intensity, color purity and quantum efficiency [4]. In order to acquire the full potential of luminescent

*) **Corresponding author:** lojpur@vinca.rs

performances, an appropriate combination of host and dopant i.e. activator must be established [5,6].

Binary rare earth oxides with general formula ARE_2O_4 (A = Ca, Sr, Ba, RE = trivalent rare earth elements) are gathering significant importance for examining luminescent properties due to their specific optical, thermal and magnetic properties [7,8]. Particularly, for us is interesting $SrGd_2O_4$, although it has shown some very promising properties such as good charge stability, excellent thermal stability, refractive index (n≈2), high density (~7.3 g/cm^3) and high chemical robustness, it has not been extensively researched [9-15]. For these reasons, along with its high-chemical stability and environmental-friendly characteristics, $SrGd_2O_4$ represents an excellent candidate for an acceptable host material [13,16]. Also, some authors indicated that the luminescent properties of a host material can be improved by incorporating various metal ions. Wang et al. investigated photoluminescence properties of $SrGd_2O_4:Eu^{3+}$ red phosphor synthesized by high-temperature solid-phase method [8]. The authors experimented with various doping concentrations of Eu^{3+} (1-15 at%) and achieved the best red emission at 611 nm, caused by $^5D_0 \rightarrow {}^7F_2$ transition (λ_{ex}=267 nm) at 5at% Eu^{3+} dopant concentration. Singh et al. [10] synthesized $SrGd_2O_4:Eu^{3+}$ phosphors *via* homogeneous precipitation method followed by the combustion process and experimented with different dopant concentrations (1-7 mol% Eu^{3+}) as well as with different processing temperatures (800-1200^{o}C) developing phosphors with strong red emission at 615 nm (λ_{ex}=264 nm). Sun et al. [11] analyzed luminescence properties of scintillating phosphors based on $SrGd_2O_4$ doped with Eu^{3+} and Dy^{3+}, synthesized by the solid-state reaction. Emission spectra of the $SrGd_2O_4:Dy^{3+}$ phosphors showed strong blue and yellow emission peaks at 490 and 580 nm, respectively, $SrGd_2O_4:Eu^{3+}$ showed emission peaks at 581, 593, 616, 657 and 710 nm, while co-doping with both Eu^{3+} and Dy^{3+} enabled them to observe energy transfer from Dy^{3+} to Eu^{3+} ions. Zhang et al. [13] prepared their samples doped with $Eu^{3+}$and Tb^{3+} ions by the solid-state reaction, and observed that Eu^{3+} ions provided a typical red emission, whilst Tb^{3+} doped sample demonstrated green emission. In the presented literature all examples are down-conversion (DC) phosphors, since the energy transfer occurs by following mechanism: a high-energy photon is converted into two (or more) low energy photons [17]. For preparing our samples combustion method was chosen due to the lower temperature requirement and higher cost-effective ratio [18].

To the best of our knowledge, so far only two papers have proposed a synthetic route and analysis of luminescent properties of $SrGd_2O_4:Dy^{3+}$[10,13] and no manuscripts published on $SrGd_2O_4:Sm^{3+}$phosphors. The motivation for the selection of dopant ions for our system is as follows: Dy^{3+} ions are expected to give enhanced blue ($^4F_{9/2} \rightarrow {}^6H_{15/2}$ transition, ≈490 nm) and yellow emission ($^4F_{9/2} \rightarrow {}^6H_{13/2}$ transition, ≈580 nm) [2, 5, 9] while Sm^{3+} is supposed to give yellow ($^4G_{5/2} \rightarrow {}^6H_{13/2}$ transition, ≈570 nm), orange ($^4G_{5/2} \rightarrow {}^6H_{7/2}$ transition, ≈600 nm) and red emission ($^4G_{5/2} \rightarrow {}^6H_{9/2}$ transition, ≈650 nm) [3,4,6]. In this work, for the first time, we present Sm^{3+} and Dy^{3+} doped $SrGd_2O_4$ phosphors synthesized *via* glycine-modified combustion method assisted with structural, morphological and luminescence characteristics of as-synthesized nanopowders were investigated as well as the influence of various dopant concentrations.

2. Materials and Experimental Procedures

2.1 Synthesis procedure

Chemicals used without previous purification for synthesis were strontium nitrate (Puratonic 99.9 %), gadolinium nitrate hexahydrate (Acros Organics 99.9 %), dysprosium nitrate pentahydrate (Sigma Aldrich, 99.9 %), samarium nitrate hexahydrate (Acros Organics 99.9 %), citric acid (Kemika 99 %) and glycine (Kemika 99.5 %).

$SrGd_2O_4$ doped with Dy^{3+} (1, 3, 5 and 7 at%) and Sm^{3+} (0.25, 0.5, 1 and 2 at%) were synthetized by the citrate sol-gel method with glycine as a fuel, followed by thermal treatment in air. Firstly, gadolinium nitrate hexahydrate, $Gd(NO_3)_3$*$6H_2O$ was dissolved in deionized water together with dysprosium nitrate hexahydrate, $Dy(NO_3)_3$*$6H_2O$ or samarium nitrate hexahydrate $Sm(NO_3)_3$*$6H_2O$ and strontium nitrate, $Sr(NO_3)_2$ was dissolved separately. The next step of the synthesis was addition of citric acid to both solutions, which were then left on a hot plate with constant magnetic stirring for half an hour. Then the solutions were mixed, glycine [NH_2CH_2COOH] was added to the solution, and the temperature was increased to 120ºC. After approximately 1 h a wet gel was produced and subsequently burned in the furnace at 500ºC for 1.5 h. Finally, the samples were calcined for 2 h at 1000ºC.

2.2 Characterization methods

The phase composition of thermally treated Sm^{3+} and Dy^{3+} activated $SrGd_2O_4$ powders was determined using X-ray diffraction (Rigaku Ultima IV, Japan). The X-ray beam was nickel-filtered Cu$K\alpha_1$ radiation (λ = 0.1540 nm, operating at 40 kV and 40 mA). The XRD data were collected from 20 to 70^o (2θ) with the 0.02 step size at a scanning rate of 5^o/min.

The samples for TEM investigation were prepared by dispersing the powder in ethanol, and after dispersion a drop of the solution was placed on a carbon-coated copper grid and dried in air. Structural characterization of the samples was done by transmission electron microscopy (TEM) in conventional and high-resolution modes, using an FEI Talos F200X microscope (Thermo Fisher Scientific, 168 Third Avenue,Waltham, MA USA) operated at 200 keV. To investigate the presence of dopant ions in samples, energy-dispersive X-ray spectroscopy (EDX) was performed.

Photoluminescent properties measurements of the Sm^{3+} samples were taken on a Horiba Jobin Yvon Fluorolog FL3-22 spectrofluorometer at room temperature, with a Xe lamp as the excitation light source. The luminescence spectra of the Dy^{3+} doped samples were measured with SpexFluorolog spectrofluorometer with Xenon lamp as the excitation source.

3. Results and Discussion

3.1. X-ray powder diffraction (XRD)

Fig. 1. presents XRD diffractograms of $SrGd_2O_4$ doped with different concentrations of Dy^{3+} (1, 3, 5 and 7 at%) and Sm^{3+} (0.25, 0.5, 1 and 2 at%). The XRD analyses showed that all samples crystallize as single phase and all diffraction peaks are well indexed to the orthorhombic lattice $SrGd_2O_4$ (space group *Pnma*, JCPDS Card No.:01-072-6387, ICSD: 96232). Change in the peak position was not observed, suggesting that the incorporation of dopant ions didn’t affect the crystal structure. Unit cell parameters (a, b, c) were calculated from XRD patterns and are presented in Table 1. The structure of $SrGd_2O_4$ is comprised of dodechacedron SrO_8 aligned with *a*-axis and double octahedral Gd_2O_4 framework with channels propagating parallel to the *c*-axis. Samples doped with Dy^{3+} showed shrinkage of unit cell in the *c*-direction suggests that the Gd^{3+} ions are replaced by smaller dopant ion (Gd^{3+}= 0.938Å, Dy^{3+}=0.912 Å). In the case of Sm^{3+} (Sm^{3+}= 0.958 Å), small amounts of dopant didn’t influence the size of unit cell, since the change of unit cell parameters are negligible.

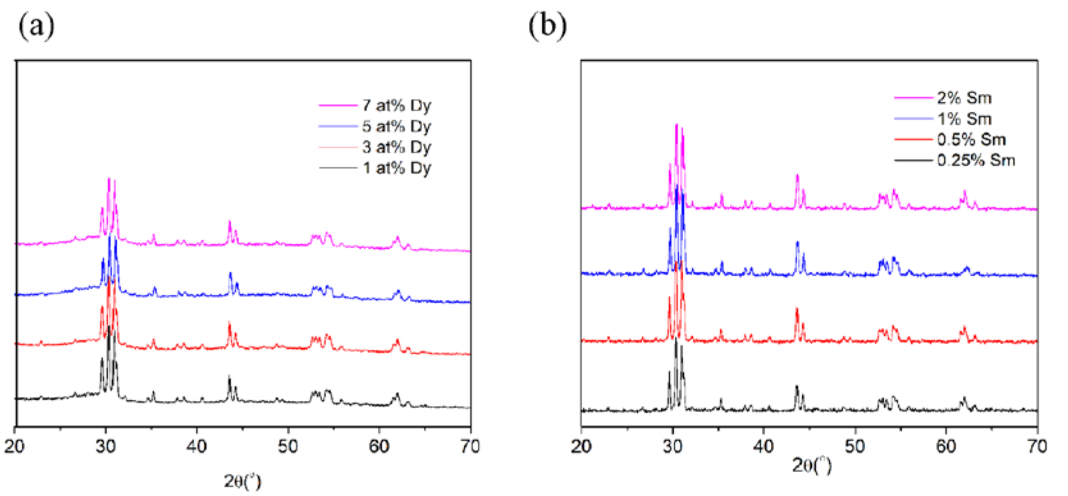

Fig. 1. XRD patterns of $SrGd_2O_4$ doped with different concentrations of a) Dy^{3+} (1, 3, 5 and 7 at%) and b) Sm^{3+} (0.25, 0.5, 1 and 2 at%).

Tab. I Lattice parameters (*a*,*b*,*c*) of $SrGd_2O_4$ doped with different amounts of Dy/Sm.

	***a* (Å)**	***b* (Å)**	***c* (Å)**
1 at% Dy	10.126 (8)	3.472(3)	12.069(16)
3 at% Dy	10.125419	3.476222	12.059116
5 at% Dy	10.111534	3.471762	12.042487
7 at% Dy	10.119769	3.476988	12.049204
0.25 at% Sm	10.086(16)	3.466(5)	12.058(19)
0.5 at% Sm	10.113(13)	3.464(2)	12.038(11)
1 at% Sm	10.10(3)	3.460(3)	12.031(14)
2 at% Sm	10.119(9)	3.465(3)	12.023(13)

3.2. Transmission-electron microscopy (TEM) investigation

For further analysis, grain size and crystallinity of obtained powders were investigated by TEM. Samples with the highest concentration of dopants (7at% Dy and 2 at% Sm) were chosen. Fig. 2. presents sample with 7 at% Dy with the grain size of approximately 200 nm, where HRTEM confirmed high crystallinity (Fig. 2b), and the lattice spacing of 0.28 nm which corresponds to (104) d-spacing (JCPDS Card No.: 01-072-6387, ICSD: 96232). Fig. 3. presents sample with 2 at% Sm where grain size is up to 150 nm with high crystallinity (Fig. 3b). Selected area electron diffraction (SAED) of both samples (Fig. 2c and 3c) confirmed presence of diffraction ring associated with (004), (302), (410) and (206) crystallographic planes of $SrGd_2O_4$ phase, confirming that the pure phase was successfully synthesized. The EDS analyses confirmed presence of Sr, Gd and O in both samples. However, because of small concentration of Sm, the presence of this dopant wasn't confirmed, and in the case of Dy, small energy peaks (Fig. 2d.) indicated by arrows could be observed confirming that single phase $SrGd_2O_4$ with incorporation of the dopant in matrix crystal structure was synthetized.

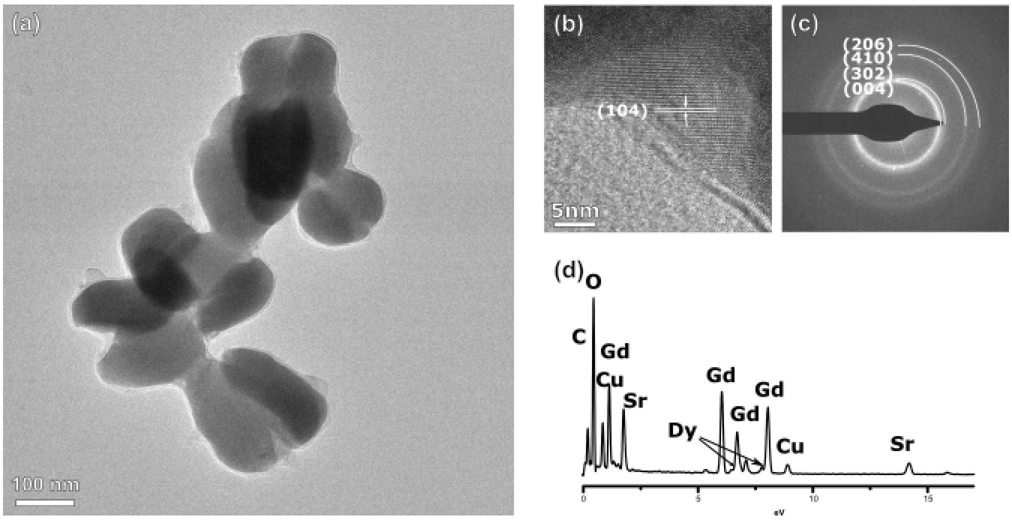

Fig. 2. TEM investigation of 7 at% Dy^{3+} co-doped $SrGd_2O_4$ particles: a) agglomerate at low magnifications; b) HRTEM image with (104) lattice planes; c) SAED of $SrGd_2O_4$ d) EDS Dy^{3+} co-doped $SrGd_2O_4$ nanoparticles.

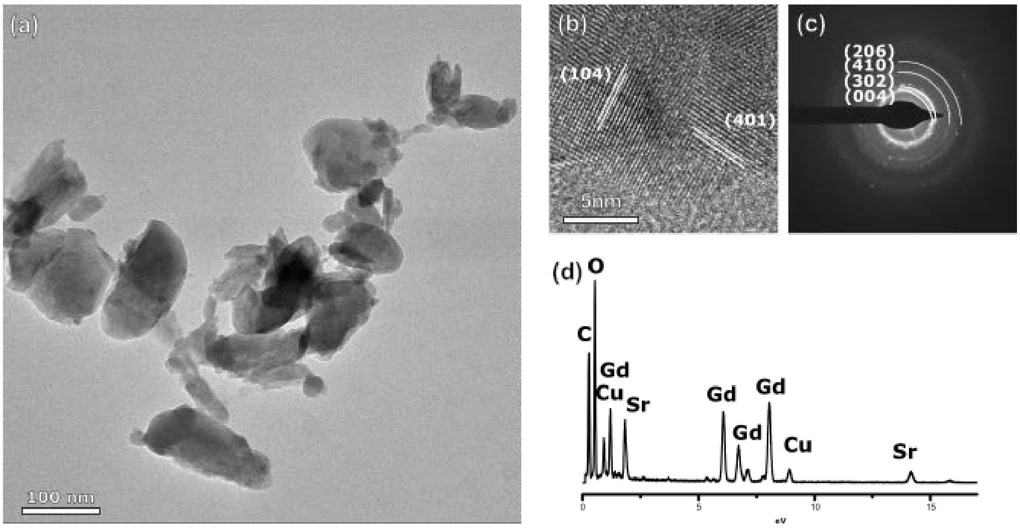

Fig. 3. TEM investigation of 2 at% Sm^{3+} co-doped $SrGd_2O_4$ particles: a) agglomerate at low magnifications; b) HRTEM image with (104) and (401) lattice planes; c) SAED of $SrGd_2O_4$ d) EDS Sm^{3+} co-doped $SrGd_2O_4$ nanoparticles.

3.3. Luminescent properties

Fig. 4. illustrates the luminescence excitation and emission spectra of Dy^{3+} doped $SrGd_2O_4$ samples recorded under room temperature. One representative excitation spectrum (3 at% Dy^{3+}) obtained with emission at 578 nm is placed in Fig. 4a, while emission spectra, obtained with excitation of 315 nm, with different concentrations of Dy^{3+} are shown in Fig. 4b. The emission spectra of the phosphors recorded at 315 nm excitation wavelength exhibit two dominating emissions at 490 and 581 nm, corresponding to $^4F_{9/2}\rightarrow{}^6H_{15/2}$ and $^4F_{9/2}\rightarrow{}^6H_{13/2}$ transitions, respectively. The $^4F_{9/2}\rightarrow{}^6H_{15/2}$ transition is magnetic dipole transition and so less sensitive to the coordination environment. The $^4F_{9/2}\rightarrow{}^6H_{13/2}$ transition belongs to a forced electric dipole transition, which is allowed only in the case that the Dy^{3+} ions are located at

the local sites with non-inversion center symmetry. Although f→f transitions are forbidden by the Laporte parity rule, most of the transitions in $(RE)^{3+}$ ions occur at the electric dipole (ED) order due to the admixture of the $4f^n$ states with opposite parity excited states $4f^{n-1}5d$, as a result of the lack of inversion symmetry [19-21]. Comparing the intensity of emissions, it can be said that the yellow emission ($^4F_{9/2}\rightarrow{}^6H_{13/2}$) is stronger than the blue emission ($^4F_{9/2}\rightarrow{}^6H_{15/2}$), indicating that Dy^{3+} is located in a more non-centrosymmetric position in the $SrGd_2O_4$ host. Several samples were prepared in order to investigate the optimum dopant concentration in this host matrix. As one can see the highest intensity is obtained with the lowest dopant concentration and a further increase in Dy^{3+} concentration subsequently decreases the peak intensity.

The schematic energy-level diagram together with the CIE diagram of Dy^{3+} doped $SrGd_2O_4$ are depicted in Fig. 5. Looking at Fig. 5a it is observable that after excitation at 315 nm Dy^{3+} ions are promoted to the $^4M_{17/2}$ state and afterward non-radiative transition to $^4F_{9/2}$, blue (at 490 nm, $^6H_{15/2}$) and yellow (at 581 nm, $^6H_{13/2}$) emission are visible [20]. As a consequence, the Commission International del' Eclairage (CIE) chromaticity coordinates, determined from emission spectra alter as it is shown in Fig. 5b. The X, Y values of (0.44, 0.42), (0.44, 0.42), (0.36, 0.35), and (0.35, 0.35) are determined for 1, 3, 5 and 7 at% of Dy^{3+} doped $SrGd_2O_4$, respectively. Samples with 1 and 3, as well as 5 and 7 at%, have the same and almost the same coordinates, implying that concentration of dopant equivalent to or higher than 5 at% leads to the emission shifting.

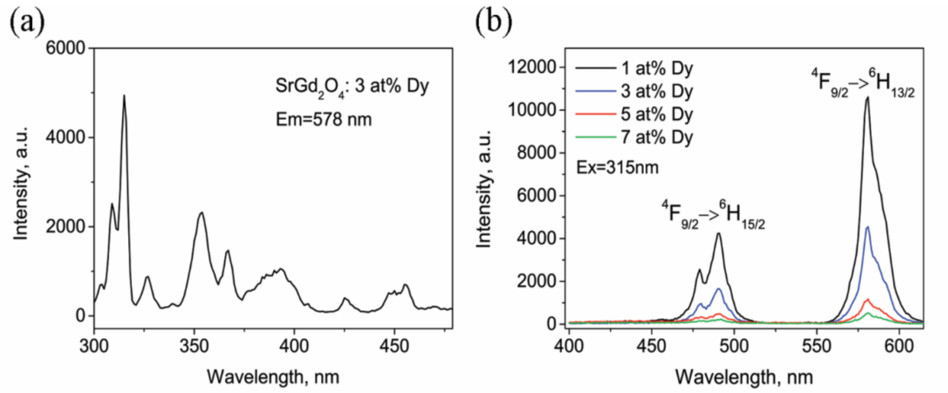

Fig. 4. Excitation (a) and emission (b) spectra of Dy^{3+} doped $SrGd_2O_4$.

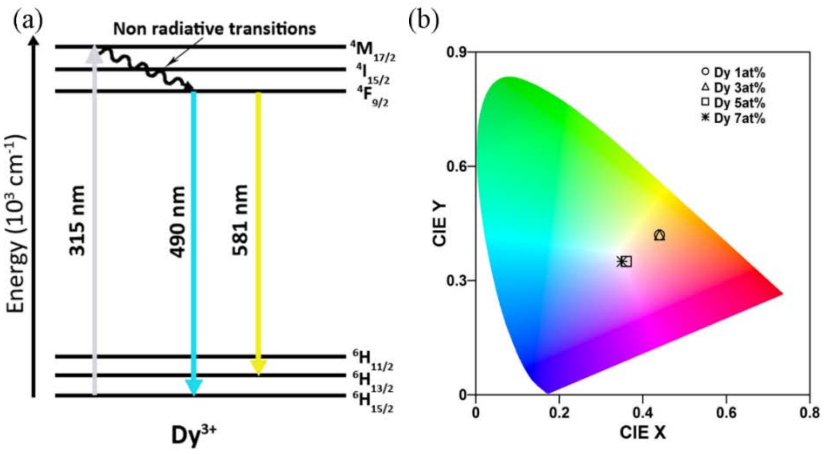

Fig. 5. Schematic energy-level diagram with characteristic emissions (a) and CIE diagram (b) of Dy^{3+} doped $SrGd_2O_4$.

The luminescence excitation and emission spectra of Sm^{3+} doped $SrGd_2O_4$ samples recorded at room temperature are shown in Fig. 6. One representative excitation spectrum (1 at% Sm^{3+}) obtained with emission at 614 nm is placed in Fig. 6a, while emission spectra, obtained with excitation of 407 nm, with different concentrations of Sm^{3+} are shown in Figure 6b. In the emission spectra, one can see the characteristic peaks of Sm^{3+} ions at 575, 615 and 655 nm which corresponds to the appropriate energy transitions from $^4G_{5/2}$ to yellow $^6H_{5/2}$, orange $^6H_{7/2}$ and red $^6H_{9/2}$ emissions, respectively. It is obvious that transition $^4G_{5/2}\rightarrow{}^6H_{7/2}$ have the most prominent intensity, comparing with the other transition bands, which is in good relation with the literature data [22,23]. Moreover, it is noticed that the concentration of dopant significantly influences the intensity of emission spectra, so with the lowest concentration of Sm^{3+} (0.25 at%), the persuasively highest emission intensity is obtained.

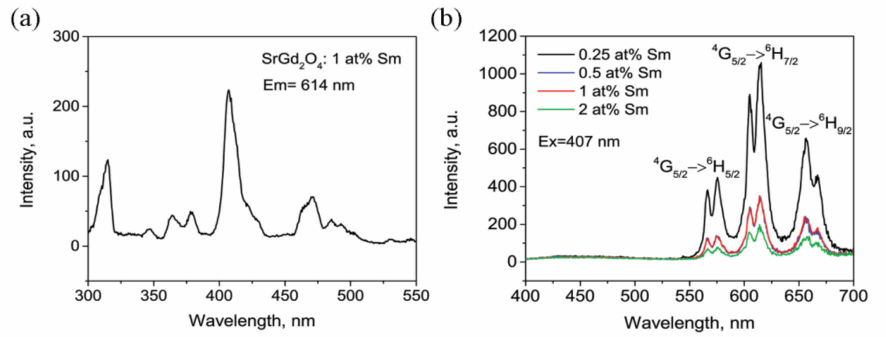

Fig. 6. Excitation (a) and emission (b) spectra of Sm^{3+} doped $SrGd_2O_4$.

The schematic energy-level diagram with visible emissions and CIE diagram for the Sm^{3+} doped $SrGd_2O_4$ phosphor are presented in Fig. 7. One can see that after the ions of Sm^{3+} are pumped with the excitation at 407 nm, they are promoted to the $^6P_{3/2}$ state and afterwards non-radiative transition to $^4G_{5/2}$, yellow (at 575 nm), orange (at 615 nm) and red (at 655 nm) emissions are visible. As in the case of Dy^{3+}, the Commission International del' Eclairage (CIE) chromaticity coordinates for Sm^{3+} was determined from emission spectra alter as it is shown in Fig. 7b.

The X, Y values of (0.57, 0.37), (0.51, 0.35), (0.52, 0.35), and (0.48, 0.34) are determined for 0.25, 0.5, 1 and 2 at% of Sm^{3+} doped $SrGd_2O_4$, respectively. Variation in dopant concentration evidently shifts the emission color, and with the 0.25 at% of Sm^{3+}, the most intense orange color is obtained.

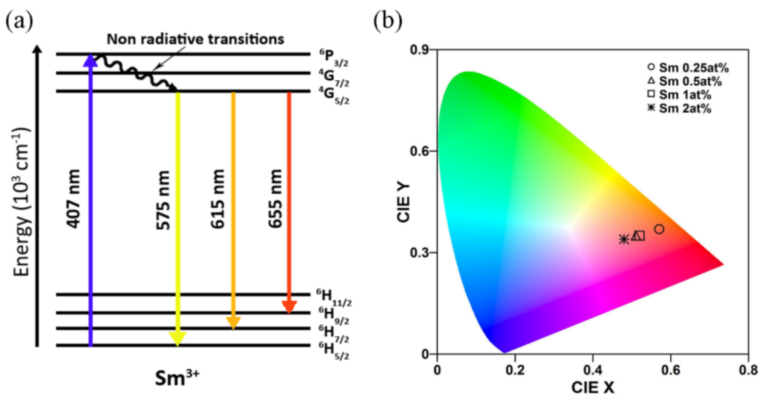

Fig. 7. Schematic energy-level diagram with characteristic emissions (a) and CIE diagram (b) of Sm^{3+} doped $SrGd_2O_4$.

4. Conclusion

Two newly down-conversion $SrGd_2O_4$ based luminescent material doped with different concentrations of Dy^{3+} and Sm^{3+} was prepared by the combustion method with glycine as fuel and citric acid as a chelator. The XRD of all obtained samples confirmed that single phase orthorhombic $SrGd_2O_4$ was successfully synthesized. Calculated lattice parameters showed that dopants were successfully incorporated in the crystal lattice of the host. We confirmed that by incorporation of Sm^{3+} ions in $SrGd_2O_4$ matrix, emission spectra demonstrated three characteristic peaks that are assigned to the $^4G_{5/2}$ to yellow $^6H_{5/2}$, orange $^6H_{7/2}$ and red $^6H_{9/2}$ transitions, placed at 575, 615 and 655 nm, respectively. Emission spectra for the samples doped with Dy^{3+} showed two dominant characteristic peaks that correspond to blue $^4F_{9/2}\rightarrow{}^6H_{15/2}$ and yellow $^4F_{9/2}\rightarrow{}^6H_{13/2}$ emissions, found at 490 and 581 nm, respectively. Also, investigation of optimum dopant concentration showed that in both cases (Dy^{3+} and Sm^{3+}) the lowest concentration provides the highest luminescent intensity and that these samples exhibit ability for emission color tuning.

Acknowledgments

The research was funded by the Ministry of Education, Science and Technological Development of the Republic of Serbia on the research program grant No. 0402211, Vinča Institute of Nuclear Sciences, National Institute of the Republic of Serbia, University of Belgrade, Serbia.

5. References

1. B. Tian, B. Chen, Y. Tian, X. Li, J. Zhang, J. Sun, H. Zhong, L. Cheng, S. Fu, H. Zhong, Y. Wang, X. Zhang, H. Xia and R. Hua,J. Mater. Chem. C, 2013 (1) 2338-2344.
2. Lj. Miličić, A. Terzić, L. Pezo, N. Mijatović, I. Brčerski, N. Vukelić, Sci. Sint. 53 (2021) 169-185.
3. L. Yu, F. Hong, Y. Wang, H. Xu, G. Liu, X. Dong, J. Wang and W. Yu, J. Lumin., 222 (2020) 117155.
4. H.-R. Shih, Y.-Sh. Chang, Material., 2017 (10) 779.
5. V. Lojpur, Ž. Antić, R. Krsmanović, M. Medić, M. G. Nikolić, M. D. Dramićanin, J. Serb. Chem. Soc., 2012(77) 1735–1746.
6. V. Mahalingam, J.Thirumalai, R. Krishnan, S.Mantha, Spectrochim. Acta A Mol. Biomol. Spectrosc., 152 (2016) 172-180.
7. R. Priya, S. Kaur, U. Sharma, O. P. Pandey, S. J. Dhoble, J. Mater. Sci. Mater. Electron., 31 (2020) 13011-13027.
8. V. Lojpur, S. Stojanović, M. Mitrić, Sci. Sinter., 50 (2018) 347-355.
9. J.-F. Wang, H. Zu, C.-W. Lin, S.-J. Ding, P.-Y. Shao,Y. Xia, Inter. J. Optic., 2020 (2020) 3095429.
10. J. Singh, P. Kr. Baitha, J. Manam, J. Rare Earth., 33 (2015) 1040-1050.
11. X.-Y. Sun, T.-T. Han, D.-L. Wu, F. X., S.-L. Zhou, Q.-M. Yang, J.-P. Zhong, J.Lumin., 204 (2018) 89-94.
12. Jyoti Singh, J. Manam, Ceram. Int., 42 (2016) 18536-18546.
13. J. Zhang, Y. Wang, L. Guo, Y. Huang, J. Am. Ceram. Soc., 95 (2012) 243-249
14. Jun-Feng Wang, Hao Zu, Chuan-Wen Lin, Shou-Jun Ding, Peng-Yu Shao and Ye Xia, International Journal of Optics, 2020 (2020) 3095429.
15. J. Singh, J. Manam, F. Singh, Mater. Res. Bull.,93 (2017) 318-324

16. J. Singh, J. Manam, Mater. Res. Bull., 88 (2017) 105-113.
17. L. Mariscal-Becerra, V. M. Velazquez-Aguilar, M. C. Flores-Jimenez, D. Acosta-Najarro, V. Torres-Zúniga, R. Vaquez-Arreguín, E. F. Huerta, H. Felix-Quintero, C. Falcony-Guajardo, H. Murrieta S, J. Alloy. Compd., 846 (2020) 156295.
18. N. M. Deraz, Sci. Sint., 53 (2021) 155-167.
19. J. Garcia Sole, L. E. Bausa and D. Jaque, An Introduction to the Optical Spectroscopy of Inorganic Solids, John Wiley and Sons Ltd., West Sussex 2005.
20. Z. Yang, H. Dong, X. Liang, C. Hou, Lipeng Liu, Fachun Lu, Dalton Trans., 30 (2014) 11474-11477.
21. G. B. Nair, S. J. Dhoble, RCS Advances, 2015 (5) 49235-49247.
22. S. Q. Mawluda, M. M. Ameen, Md. Rahim Saharb, K. F. Ahmed, J. Lumin. 190 (2017) 468-475.
23. K. Swapna, Sk. Mahamuda, A. Srinivasa Rao, S. Shakya, T. Sasikala, D. Haranath, G. V. Prakash, Spectrochim. Acta A Mol. Biomol. Spectrosc., 125 (2014) 53-60.

Сажетак: *У овом раду, детаљно су испитани „down“- конверторски нанопрахови $SrGd_2O_4$ допирани различитим концентрацијама Dy^{3+} и Sm^{3+}. Сви узорци су припремљени методом сагоревања уз помоћ глицина, првенствено спаљени на 500 степени током 1.5 сат а затим термички третирани на 1000 степени 2 сата на собној температури. Анализа дифракције зрака (XRD) је показала да сви узорци кристалишу као једнофазна и орторомбичка решетка $SrGd_2O_4$. Анализом трансмисионе електронске микроскопије (TEM) утврђен је висок степен кристалиничности узорака величине зрна од приближно 200 nm за Dy^{3+} допиране и 150 nm за Sm^{3+} допиране узорке $SrGd_2O_4$. За оба узорка SAED је потврдио да дифракциони прстенови одговарају индексима hkl равнима $SrGd_2O_4$, док је EDS потврдио присуство Dy у кристалној структури. Резултати луминисцентне карактеризације показали су све одговарајуће емисионе пикове који се односе на Dy^{3+} или Sm^{3+} допантне јоне. Испитивање концентрације допанта показало је да најниже вредности оба допанта имају најистакнутије емисионе пикове, док координате добијене из CIE дијаграма показују померање емисије са променом концентрације.*
Кључне речи: *"down" конверзија, луминесценција, $SrGd_2O_4$, синтеза сагоревања.*